

Space Weather

RESEARCH ARTICLE

10.1029/2020SW002571

Key Points:

- A new capability for measuring total electron content (TEC) from the ocean surface is presented
- First measurements of TEC from two surface buoys in the Pacific Ocean are described
- TEC enhancements in the equatorial region during moderate geomagnetic storms are observed

Correspondence to:

I. Azeem,
iazeem@astraspace.net

Citation:




Azeem, I., Crowley, G., Forsythe, V. V., Reynolds, A. S., Stromberg, E. M., Wilson, G. R., et al. (2020). A new frontier in ionospheric observations: GPS total electron content measurements from ocean buoys. *Space Weather*, 18, e2020SW002571. <https://doi.org/10.1029/2020SW002571>

Received 22 JUN 2020

Accepted 26 AUG 2020

Accepted article online 1 SEP 2020

A New Frontier in Ionospheric Observations: GPS Total Electron Content Measurements From Ocean Buoys

Irfan Azeem¹ , Geoff Crowley¹ , Victoriya V. Forsythe¹, Adam S. Reynolds¹ , Erik M. Stromberg¹, Gordon R. Wilson², and Craig A. Kohler³

¹Atmospheric & Space Technology Research Associates LLC, Louisville, CO, USA, ²Air Force Research Laboratory, Kirtland AFB, Albuquerque, NM, USA, ³National Oceanic and Atmospheric Administration, National Data Buoy Center, Stennis Space Center, MS, USA

Abstract Ground-based Global Navigation Satellite System (GNSS) receivers have become a ubiquitous tool for monitoring the ionosphere. Total electron content (TEC) data from globally distributed networks of ground-based GNSS receivers are increasingly being used to characterize the ionosphere and its variability. The deployment of these GNSS receivers is currently limited to landmasses. This means that 7/10 of Earth's surface, which is covered by the oceans, is left unexplored for persistent ionospheric measurements. In this paper, we describe a new low-power dual-frequency Global Positioning System (GPS) receiver, called Remote Ionospheric Observatory (RIO), which is capable of operating from locations in the air, space, and the oceans as well as on land. Two RIO receivers were deployed and operated from the Tropical Atmosphere Ocean buoys in the Pacific Ocean, and the results are described in this paper. This is the first time that GPS receivers have been operated in open waters for an extended period. Data collected between 1 September 2018 and 31 December 2019 are shown. The observed TEC exhibits a clear seasonal dependence characterized by equinoctial maxima in the data at both locations. Both RIO receivers, deployed near the magnetic equator, show an 18–35% increase in TEC during moderately disturbed geomagnetic periods. Comparisons with the International Reference Ionosphere model show good agreement. The new capability presented in this paper addresses a critical gap in our ability to monitor the ionosphere from the 70% of the Earth's surface that is covered by water.

Plain Language Summary The upper levels of the atmosphere, from about 80 to over 1,000 km altitudes, collectively referred to as the ionosphere, consist of partially ionized gas. An increasingly large amount of ionospheric data comes from ground-based receivers that passively benefit from the signals transmitted on board the Global Navigation Satellite System (GNSS) constellations. One of the most useful data sets provided by these GNSS receivers is the total electron content. Ground-based GNSS receivers are widely deployed all over the world and have become the workhorse for doing ionospheric research. However, to date, the deployment of these GNSS receivers has been limited to landmasses, which leaves 70% of the Earth's surface covered by the oceans uninstrumented for ionospheric studies. In this paper, we describe a new low-power dual-frequency Global Positioning System receiver, called the Remote Ionospheric Observatory, which is capable of continuous operation from ocean buoys for extended periods. We present data from two Remote Ionospheric Observatory receivers deployed on buoys in the Pacific Ocean. The new capability described in this paper is anticipated to open up many new applications for passively monitoring the ionosphere from previously inaccessible regions, such as the ocean.

1. Introduction

A significant challenge in comprehensive characterization and predictive modeling of the ionosphere is the paucity of high-fidelity and globally distributed data. The dearth of ionospheric data is most acute in the regions covered by open ocean waters. Our ability to monitor the geospace environment from the ocean remains a technological challenge. This is a problem because the oceans cover about 70% of the Earth's surface. Traditional instruments used for ionospheric monitoring, such as ionosondes, all-sky imagers, and radars are too bulky and power intensive to be deployed on resource-limited ocean buoys. Thus far, these instruments have not been demonstrated to successfully operate from buoys in open waters. Even smaller and lower-power instruments, such as dual-frequency Global Navigation Satellite System (GNSS) receivers, have not been utilized for routine ionospheric measurements from buoys. New sensor modalities that can

©2020. The Authors.

This is an open access article under the terms of the Creative Commons Attribution License, which permits use, distribution and reproduction in any medium, provided the original work is properly cited.

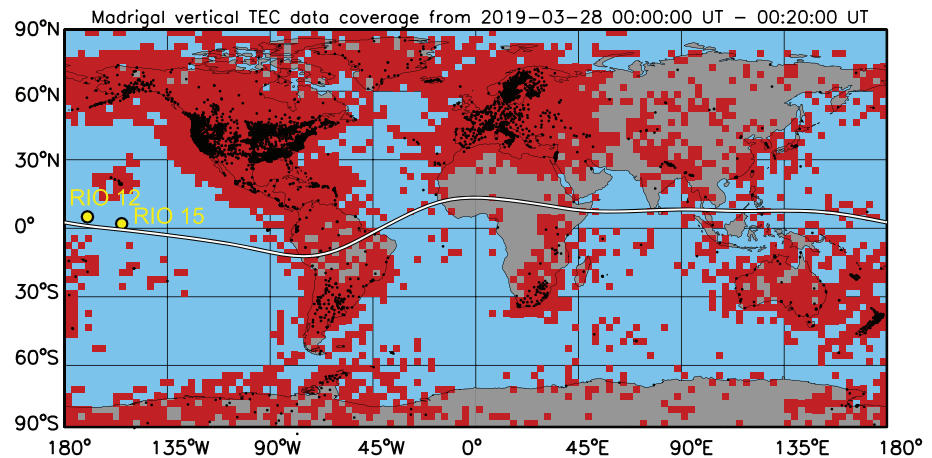


Figure 1. TEC coverage map with the locations of ionospheric pierce points (IPPs) shown in red and the locations of ground-based dual-frequency GPS receivers represented by black dots. The dearth of TEC coverage over the oceans is self-evident in the map. The yellow circles show the locations of the RIO receivers deployed on buoys. The white line is the magnetic equator. The TEC map is generated using data from the Madrigal database (<http://millstonehill.haystack.mit.edu/>).

operate from surface buoys are needed to address this critical gap in our observational capability and, if successful, will open the way for innovative research activities.

Presently, the only means to monitor the ionosphere over the oceans is from satellites. The majority of ionospheric data from space-based platforms since the 1990s has come from satellite missions in the low Earth orbit (LEO). Notable examples of satellite missions that have contributed ionospheric total electron content (TEC) or electron density profile measurements include TOPEX/Poseidon (Codrescu et al., 1999; Robinson & Beard, 1995), Constellation Observing System for Meteorology, Ionosphere, and Climate (COSMIC) (Lei et al., 2007; Schreiner et al., 2007), and now the COSMIC-2 mission (Schreiner et al., 2020). In the last few years, several commercial providers, such as Spire and GeoOptics, have also begun providing TEC/electron density profile measurements from their respective constellations of GNSS Radio Occultation satellites (Forsythe et al., 2020). Two recently launched National Aeronautics and Space Administration (NASA) missions, Ionospheric Connection Explorer (ICON) (Immel et al., 2018) and Global-scale Observations of the Limb and Disk (GOLD) (Eastes et al., 2017), are expected to provide unprecedented measurements of the ionosphere. With the exception of the GOLD mission, all of these satellite missions share one pertinent characteristic: They all are in LEO. Due to their motion relative to a fixed point on Earth, LEO satellites are unable to provide persistent observations over a given geographic location. As a result, the observed ionospheric fluctuations in the data cannot be unambiguously deconvolved and attributed to spatial and temporal geophysical variations.

Over the last decade, TEC measurements from dense networks of GNSS receivers worldwide have provided an important database to study the ionosphere. GNSS receivers have enabled researchers to create TEC maps to study ionospheric responses to geomagnetic and lower atmospheric disturbances (Azeem & Barlage, 2017; Azeem et al., 2017; Coster et al., 2017; Crowley et al., 2016; Komjathy, 1997; Mannucci et al., 1998; Occhipinti et al., 2013; Saito et al., 1988; Tsugawa et al., 2007). To date, these networks of GNSS receivers have only been deployed on land. This state of affairs is represented in Figure 1, which shows the current typical TEC coverage (red pixels) from publicly available ground-based dual-frequency Global Positioning System (GPS) receivers (black circles). Figure 1 also shows the locations of the two GPS receivers, called Remote Ionospheric Observatory (RIO), in the Pacific Ocean that are the focus of this study. We describe the RIO receiver in more detail in section 2. From the figure, it is abundantly clear that most TEC measurements come predominantly from the United States, South America, Europe, Japan, and Australia. The gaps in data coverage are primarily seen in Africa, the Middle East, Asia, Antarctica, and the oceans. In this paper, we present a new capability for ionospheric remote sensing using GPS receivers designed specifically for operation from ocean buoys that could potentially be deployed globally.



Figure 2. RIO GPS receiver.

In subsequent sections, we will provide a brief description of the small size, weight, and power (SwaP) RIO science-grade GPS receiver that is capable of operating autonomously from moored or tethered buoys. We will present TEC data from the pair of RIO GPS receivers that are deployed on the National Oceanic and Atmospheric Administration (NOAA) Tropical Atmosphere Ocean (TAO) buoys in the Pacific Ocean, as indicated in Figure 1. We will compare the TEC data with the International Reference Ionosphere 2016 (IRI-2016) model (Bilitza et al., 2017) for validation. The paper is organized as follows: The RIO GPS receiver systems on the buoys are introduced in section 2; section 3 describes the TEC data collected during field tests in Hawaii and Peru and initial validation comparisons with nearby ground-based GPS receivers; section 4 discusses the TEC data from the TAO buoys collected over a 16-month period between 1 September 2018 and 31 December 2019 along with comparisons with the IRI-2016 model; section 5 summarizes

the conclusions of this study and examines the potential of ocean-based ionospheric monitoring capability for future ionospheric research.

2. RIO GPS Receiver

RIO is a dual-frequency science-grade GPS receiver that tracks the traditional L1 (1.57542 GHz) civil signal (C/A, or coarse/acquisition code) and the L2 (1.22760 GHz) civil signal, L2C. RIO builds on the heritage of the CASES (Connected Autonomous Space Environment Sensor) receiver (Crowley et al., 2011; O’Hanlon et al., 2011), providing the same functionality as the original CASES GPS receiver but in a smaller package and with reduced power consumption. The major difference between the design of the two receivers is that CASES uses a custom-designed digital signal processor board to perform all signal acquisition and tracking and computations of the navigation solution and various observables such as pseudorange, beat carrier phase, and Doppler shift, whereas these calculations are performed on a general-purpose onboard computer in RIO. The use of a low-power processor board instead of the digital signal processor allows RIO to achieve a significant reduction in power consumption compared to the CASES GPS receiver. In contrast to CASES, the RIO GPS receiver uses only 2.5 W of power, weighs 0.585 kg, and is about 4.25" × 4.5" × 2.5" in length, width, and height. The receiver tracks only GPS signals to minimize power consumption. The RIO receiver design is optimized for operations in remote locations (including ocean deployments) where power and other resources may be extremely limited. Figure 2 shows the RIO GPS receiver in its current form as a commercial product.

RIO samples the GPS L1 and L2C signals at 100 Hz and outputs fully processed TEC data nominally at 1 Hz (these data rates are programmable via a user configuration file). The amplitude (S_4) and phase scintillation (σ_ϕ) indices are also computed onboard the receiver; however, they are not presented in this paper as they are currently undergoing validation. In this study, we will focus on the TEC data from the two RIO receivers hosted on the NOAA TAO buoys.

The main RIO components include an RF front end (RFE), a so-called mezzanine board, and a processor board. Figure 3 shows the block diagram of major components of the RIO GPS receiver. The RFE handles digitization of the data from the GPS antenna. It filters, amplifies, downconverts, samples, and packetizes the raw RF data for later processing. The mezzanine board includes a field-programmable gate array for processing and a DC/DC converter for power management. The field-programmable gate array reads the raw

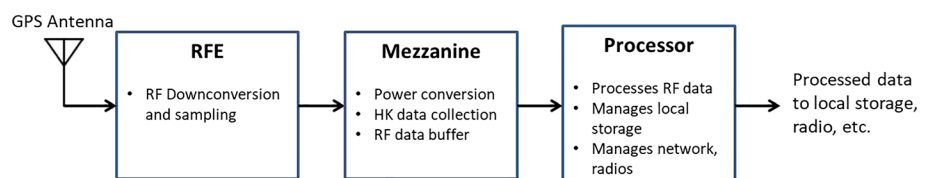


Figure 3. RIO block diagram with major components identified.

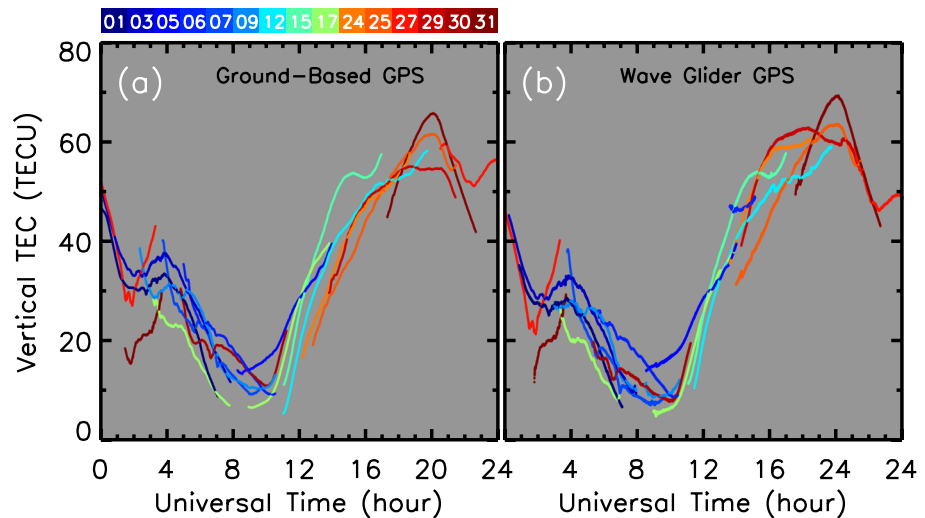


Figure 4. (a) TEC from a reference GAMMA GPS receiver located at Lima, Peru. (b) TEC from the RIO GPS receiver on the Wave Glider while deployed 22 miles off the coast of Lima. The color corresponds to the Pseudorandom noise (PRN) code of the GNSS satellite, shown on top of (a). The two time series exhibit similar trends and variations, which were interpreted as a validation of the data quality of the GPS receiver on the Wave Glider. The receiver bias in both data sets was estimated using the publicly available IONosphere-map EXchange (IONEX) global TEC data from the National Aeronautics and Space Administration (NASA) Crustal Dynamics Data Information System (<ftp://cddis.nasa.gov/gnss/products/ionex/>).

digital samples from the RFE and buffers them for the processor board. It is also programmed to collect housekeeping data such as voltages, currents, and temperatures. The DC/DC converter manages power conversion and distribution to the rest of the boards in the system. The buffered RFE data are then fed to the processor board by the mezzanine. The processor board (onboard computer) is responsible for the GPS signal acquisition, tracking, navigation, scintillation and TEC calculation, and so on. The processor board also interfaces with local data storage, network infrastructure, and any applicable communication radios, such as cell modems or satellite data modems.

3. RIO GPS TEC Field Tests and Validation

The RIO GPS receiver underwent several ocean deployments in Hawaii and Peru for functional testing, validation, and verification. These tests and evaluations of the engineering units were used to finalize the RIO design, which is now deployed on the NOAA TAO buoys. In this section, we briefly review the GPS TEC from the final field test in Peru and present comparisons of the data collected from the ocean surface to a nearby ground-based GPS receiver.

For the sea trial off the coast of Peru, a RIO engineering unit was integrated on the Wave Glider autonomous surface vehicles (Thomson et al., 2018) and deployed 22 miles (35.4 km) off the coast for 8 days under various ocean roughness conditions. The Wave Glider consists of two major systems: a floating buoy and a motor that hangs from the bottom of the buoy. The “motor” consists of a “wing” mechanism that is driven simply by wave action and can be steered by a rudder programmed from a computer on the buoy. Most of the infrastructure is contained in the floating buoy, which includes “dry-box” compartments for various payloads, a dry-box for the command and control electronics, solar panels, and various antennas. During the field test, the host Wave Glider was programmed to keep station at a reference location and telemetry signals were transmitted in real time via the Iridium satellite link to a ground site. This and previous tests (not shown here) also included a newer version of the CASES GPS receiver, called GAMMA, several of which were deployed on the ground within 1.5 miles of the shore and served to provide a stationary reference for comparisons with the measurements collected on the water.

The field test in Peru took place 20–27 January 2015, during which the host Wave Glider was programmed to perform various maneuvers that included station keeping about a reference point, straight-line transitions between two waypoints, and box pattern traversals. The TEC data shown in this section were collected on

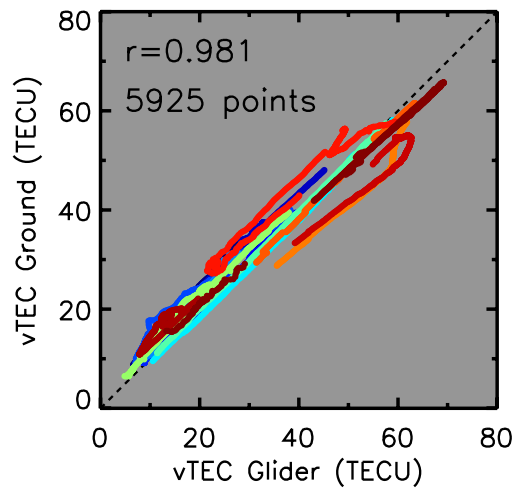


Figure 5. Comparison of vertical TEC (vTEC) measurements from the RIO GPS receiver on the Wave Glider and the reference GAMMA GPS receiver located in Lima, Peru. The colors represent different PRNs as identified in Figure 4. Each data point is a 1-min average. The correlation coefficient between a total number of 5,925 points is 0.981.

21 January 2015 when the Wave Glider was operating in a station keeping mode at 12.07°S, 77.47°W about 22 miles (~35 km) off the coast of Lima, Peru. During this test, a GAMMA GPS receiver was also deployed on the ground in Lima, Peru, at 12.05°S, 77.12°W. The L1-L2C interfrequency biases were computed for each GPS satellite in postprocessing using data products from the NASA Crustal Dynamics Data Information System (CDDIS) (Noll, 2010). Figure 4 shows the TEC measurements in units of TECU ($1 \text{ TECU} = 10^{16} \text{ \#/m}^{-2}$) from the RIO on the Wave Glider and the data from the land-based GAMMA GPS receiver in Lima. The different colored curves in Figure 4 represent several different GPS satellites tracked by the receivers. The TEC data from the land-based GAMMA are shown in Figure 4a, while the concurrently acquired RIO data are plotted in Figure 4b. The TEC measurements from RIO on the Wave Glider show good qualitative agreement with those from the reference ground-based GAMMA GPS receiver. One does not necessarily expect the two data sets to be identical since the ionosphere over Peru tends to contain a lot of variable structure, and the receivers were about 22 miles apart, resulting in a slightly different ionospheric pierce point geometry. Nonetheless, the TEC measurements from the ground-based and ocean-deployed GPS receivers show similar variations and trends in the data. The overall agreement between the two data sets suggests that the

RIO measurements from the buoy are comparable in quality to the ground-based TEC data. To better quantify this agreement, 1-min averaged TEC data from the Wave Glider and ground-based GAMMA are compared to each other in Figure 5. The correlation coefficient between the 5,925 TEC data points compared is 0.98, showing extremely good agreement. As mentioned earlier, trials were performed over an 8-day interval, and similar results were obtained every day.

4. RIO Systems on NOAA TAO Buoys in the Pacific Ocean

In August 2018, two RIO receivers, hereafter referred to as RIO-12 and RIO-15, were deployed on the NOAA TAO buoys in the Pacific Ocean near the geographic equator. The locations of these buoys are shown in Figure 1. The TAO array (Hayes et al., 1991) consists of approximately 70 moored buoys in the tropical Pacific Ocean to provide ocean and atmospheric observations in support of El Niño/Southern Oscillation monitoring and prediction. The TAO array is operated by the NOAA National Data Buoy Center (NDBC). The TAO buoys are typically deployed in water depths between 1,500 and 6,000 m, and each one consists of a 2.3-m-diameter fiberglass/foam toroid, with an aluminum tower and a stainless steel bridle (see Figure 6).



Figure 6. NOAA TAO buoy similar to those hosting RIO GPS receivers in the Pacific Ocean.

While each TAO buoy includes data logging, telemetry, and battery systems to support various meteorological and hydrographic sensors, we only used them as platforms to mechanically host the RIOs. This was done deliberately so as not to interfere with the NOAA/NDBC's mission-critical measurements. The RIO systems designed for the TAO buoys included their own telemetry, thermal management, and power subsystems, allowing them to operate autonomously and independently of the other sensors and systems. Each RIO is housed in a weather-proof and corrosion-resistant enclosure along with an Iridium communication modem, an overvoltage protection system, low-power alarms, and an advanced power management controller to protect electronic equipment from catastrophic events. A solar panel (also rated for operations in the marine environment) was mounted on each of the three vertical faces of the aluminum tower, and a GPS antenna was affixed to the top ring of the TAO buoy. Each RIO system includes the ANTCOM S5GIR1216RR-AP-XST-1-HF combined L1/L2 GPS and Iridium patch antenna mounted on top of the TAO tower. Figure 7 shows a drawing of the RIO GPS

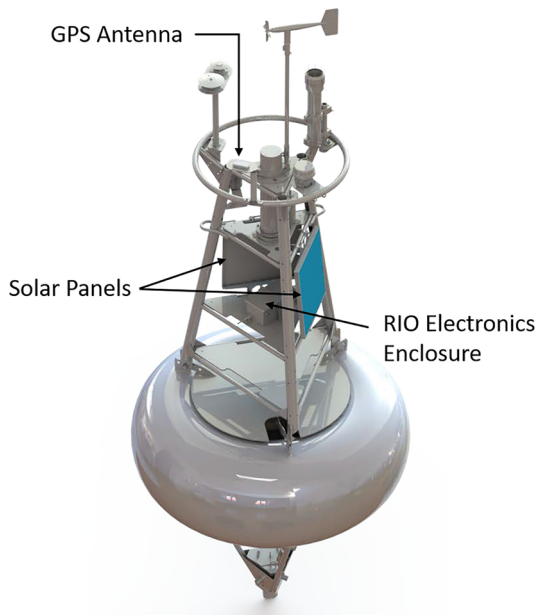


Figure 7. Computer rendering of the NOAA TAO buoy showing the placements of the RIO electronics enclosure, the GPS antenna, and two out of three solar panels.

receiver's placement on the TAO buoy. The figure also shows the locations of the GPS antenna and the solar panels. Both RIO systems operated continuously and maintenance free on the TAO buoys during the 16-month measurement period presented in this paper. It is also worthwhile to note that the RIO system software can be upgraded remotely via the Iridium connection if needed.

Fully processed 1-min resolution slant TEC (STEC) data from the RIO receivers on each of the TAO buoys are transmitted to a ground-side server over the Iridium link. The STEC data are converted to vertical TEC (ν TEC) in postprocessing using an ionospheric pierce point height of 350 km. The results presented in section 5 show ν TEC data from the RIO systems. In this paper, ν TEC and TEC are used interchangeably. The RIO data extraction strategy is as follows: Science and housekeeping data are continuously saved to a buffer on the RIO. Every 2 hr, the data are transmitted to the server, and the buffer is cleared. During routine operations, the transmitted packet would include STEC data from the last 2 hr. If for any reason, a scheduled Iridium connection is not established successfully, the RIO processor would reinitiate the connection every hour until a link is established at which point all buffered data are transmitted. The chosen connection period of 2 hr is driven entirely by the need to reduce the incurred Iridium data charges and is not an attribute of any technical requirements or impediments. If desired, the data could be returned in near real time for operational campaigns.

5. Results

In this section, we present summary plots of the TEC data from RIO-12 and RIO-15 collected between 1 September 2018 and 31 December 2019. These summary plots show 5-min averaged TEC data from all available GPS satellites. The averaging was done to reduce high-frequency noise in the TEC data. For visual clarity, we show two sets of summary plots for each RIO receiver: one plot covering 1 September through 31 December 2018 and the other for the entire year of 2019. Only TEC values obtained above 20° elevations are used in generating these summary plots. The 10.7-cm solar radio flux ($F_{10.7}$) during this observation period was representative of solar minimum conditions. The 81-day running mean of the daily $F_{10.7}$ over the data collection period is shown in Figure 8. The prevailing solar minimum conditions make this data set ideal for studying ionospheric responses to external drivers, such as geomagnetic storms.

5.1. TEC From RIO-12 and RIO-15 GPS Receivers

Figure 9 shows the local time (LT) variations of the measured TEC between 1 September and 31 December 2018 from RIO-12 and RIO-15. The figure also shows the Dst and Kp indices during the same period. It is worth reminding ourselves that RIO-12 is deployed near 5°N, while the RIO-15 host buoy is moored near 2°N. The geomagnetic latitudes of RIO-12 and RIO-15 are 3.73°N and 3.4°N, respectively. The buoys are separated by about 1,800 km in the east-west direction. While there exist subtle differences in the data from the two locations, in this section we focus on the main features of the TEC measurements that are common

to both data sets. Both receivers show the dayside increase in TEC between 10 and 18 LT, driven by the plasma generation from solar illumination. On average, the peak daytime TEC values are about 30 TECU during the equinox months (September–November) and 22 TECU during December. Figure 10 shows year-long TEC measurements from RIO-12 and RIO-15 in 2019. As with Figure 9, the daytime TEC increase is clearly evident between 10 and 18 LT in both data sets. The white regions in Figures 9 and 10 represent times when the receivers were not able to produce TEC measurements due to cycle slips experienced during rough seas as a result of the originally configured narrow phase lock loop bandwidth. We have recently updated the phase lock loop bandwidth remotely to

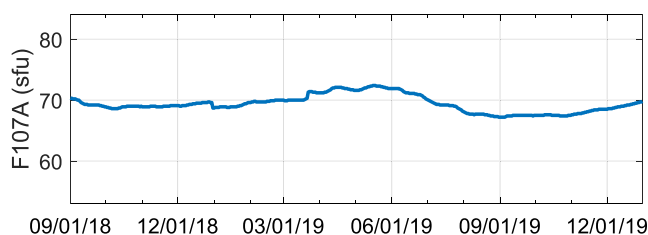


Figure 8. The 81-day running mean of the daily $F_{10.7}$ index between 1 September 2018 and 31 December 2019.

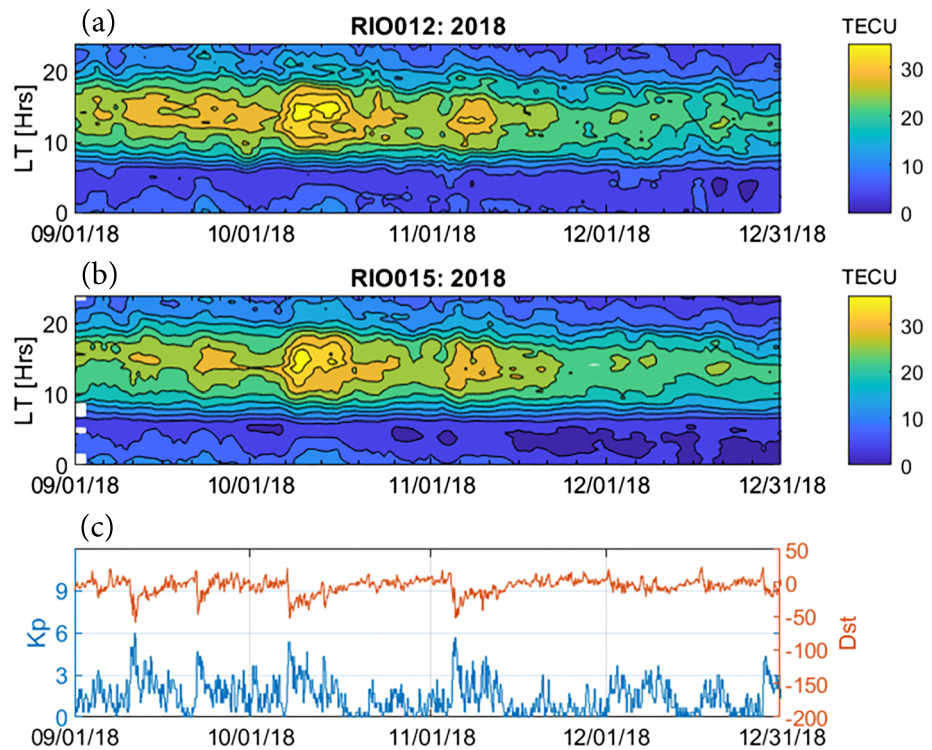


Figure 9. TEC data from (a) RIO-12 and (b) RIO-15 GPS receivers between 1 September and 31 December 2018. (c) *Dst* and *Kp* indices during this period. Several moderate storms are evident in the *Dst* and *Kp* data.

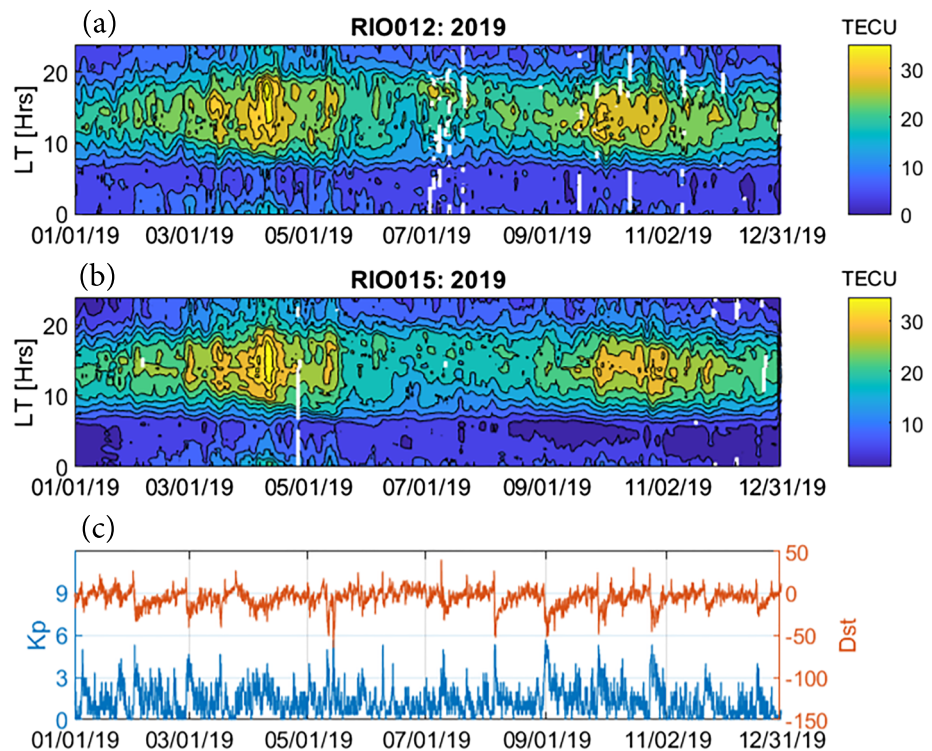


Figure 10. Same as Figure 9 but for TEC data collected between 1 January and 31 December 2019.

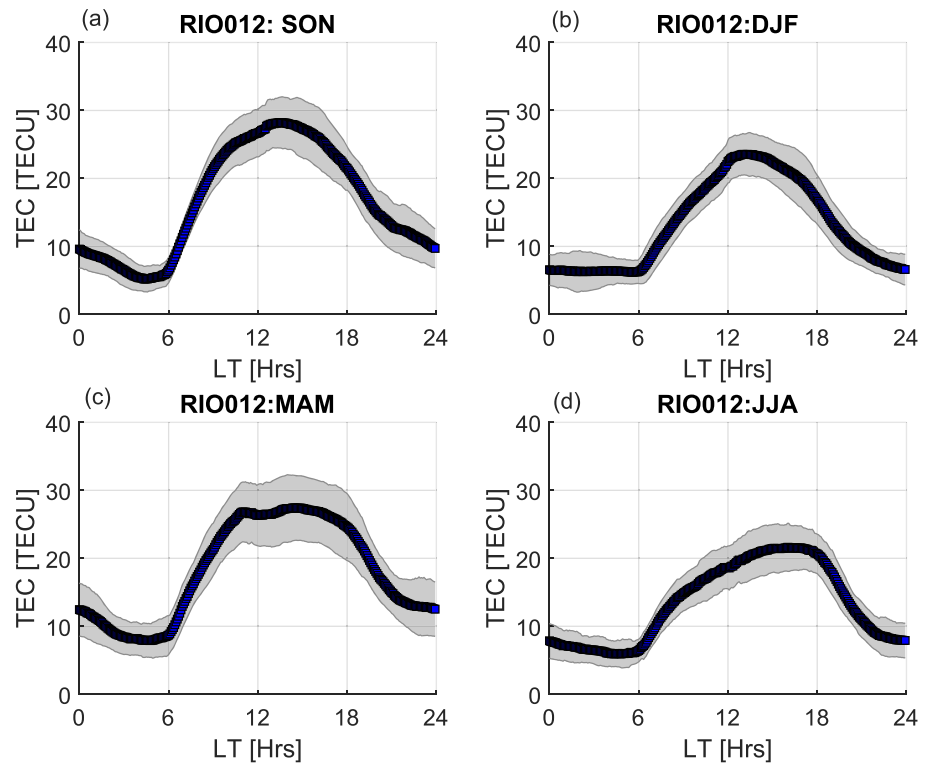


Figure 11. Seasonally averaged local time variations of TEC from the RIO-12 GPS receiver for (a) fall equinox, (b) winter solstice, (c) spring equinox, and (d) summer solstice. The gray shaded region in each of the panels represent 1σ standard deviation.

address this issue. For the TEC measurements presented in this paper, the data gaps due to cycle slips amounted to only 0.2% of the total uptime of the receivers. As a result of the software update, we expect the uptime of RIOs to be 100%. These year-long data sets also reveal clear annual, semiannual, and seasonal variations. The seasonal variation is characterized by TEC values that are lower during solstices than during the equinox months.

An inspection of the *Dst* and *Kp* data in Figures 9 and 10 reveals several moderate geomagnetic storms (*Dst* ~ -50 nT) interspersed throughout the observation period of this study. A clear association between TEC enhancements and *Dst* excursions during storm times is apparent in the figures. The TEC is seen to increase rapidly at the storm onset and remains elevated for at least several days during the recovery period. This behavior of TEC during storm times has been reported previously (Buonsanto, 1999; Heelis, 2013; Lei et al., 2014; Mannucci et al., 2005). A potential driver of the storm time increase in the dayside TEC is the eastward directed prompt penetration electric field of magnetospheric origin and the associated upward $\mathbf{E} \times \mathbf{B}$ drifts at the equator, which lifts the plasma upward and raises the layer to altitudes where recombination rates are low (Mannucci et al., 2005). Storm time thermospheric circulation and disturbance dynamo impacts can also contribute to the long-duration TEC response and cannot be ruled out (Buonsanto, 1999; Lei et al., 2014). The relative contributions of various driving mechanisms of the TEC response to geomagnetic storms, as seen in the RIO measurements, will be examined in detail in a future study.

Figure 11 shows seasonally averaged LT variations in the 5-min averaged TEC data from RIO-12. These seasonal averages were formed using all available data between September 2018 and December 2019. The gray shaded regions represent 1σ standard deviation. Comparing the peak TEC values across different panels in Figure 11, we observe that there are annual and semiannual variations with maxima near the equinoxes, a primary minimum near the June solstice, and a secondary minimum near the December solstice. Similar annual/semiannual variations have been reported in the daytime low-latitude N_mF_2 and h_mF_2 data from the COSMIC mission by Burns et al. (2012). Similar seasonal averages were computed for RIO-15, which show identical features and therefore are not shown here. There are clear differences in the LT variation

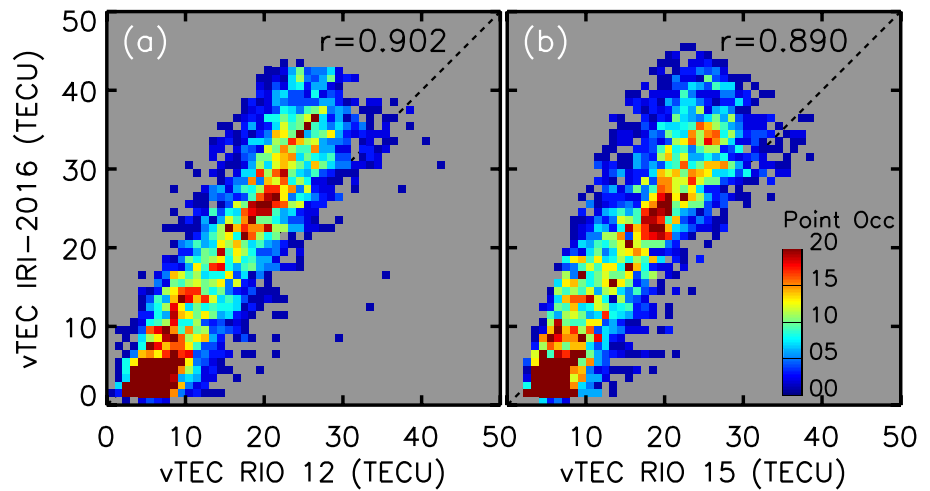


Figure 12. Comparison between hourly averaged TEC from (a) RIO-12 and (b) RIO-15 GPS receivers and IRI-2016 TEC. The colors represent different data point occurrences in accordance with the color bar shown in (b). The total number of data points compared are 5,755 and 5,771 for RIO-12 and RIO-15, respectively. The linear correlation coefficients are shown at the top of the panels.

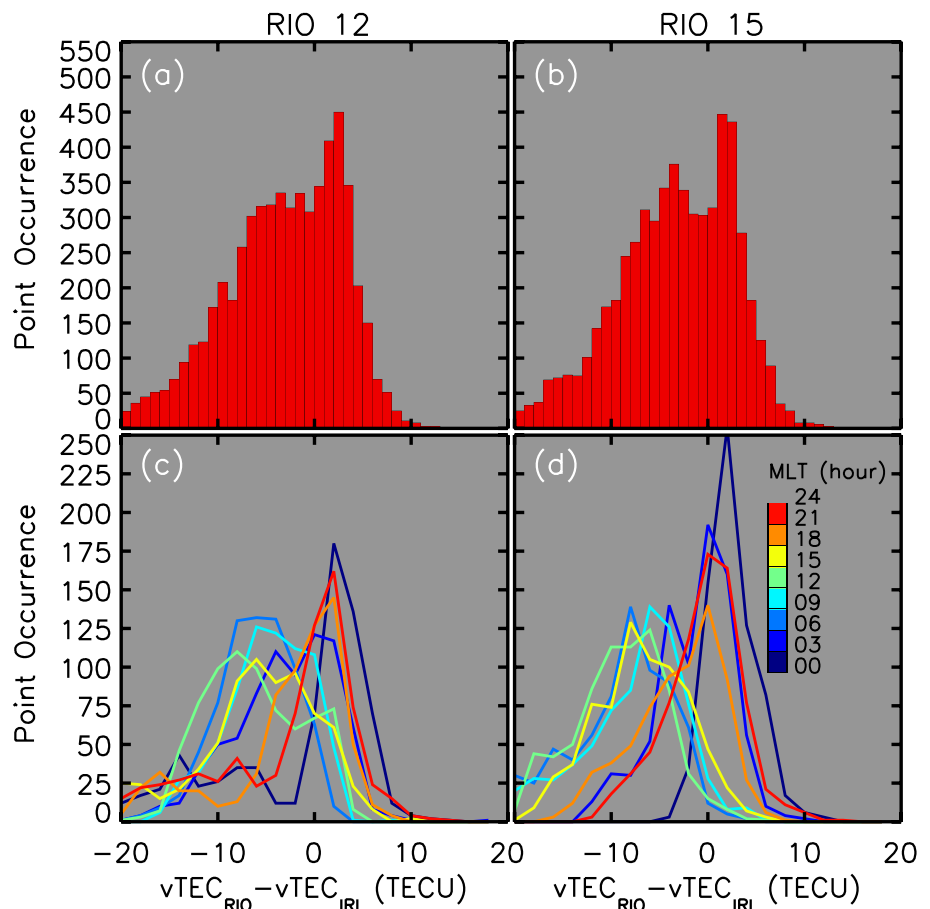


Figure 13. Differences between the TEC from the IRI-2016 model and (a) RIO-12 and (b) RIO-15. Panels (c and d) The differences binned in MLT, indicated by the color with the color bar shown in (d).

between different seasons, which will be examined in detail in a future study. Here, we simply note that the spring equinox and summer solstice daytime TEC tend to have a flatter LT response in contrast to the fall and winter daytime TEC values, which exhibit a steeper rise and roll off.

5.2. Comparisons With IRI-2016

To assess the overall data quality from the RIO receivers, we compared the RIO-12 and RIO-15 TEC measurements with the IRI-2016 (Bilitza et al., 2017). IRI-2016 is an empirical model of the ionosphere primarily based on the data from the global networks of ionosondes, incoherent scatter radar, and satellite and rocket measurements. Since it is data driven, the IRI model works best in regions with the highest density of data. It follows that IRI results over the oceans, where the data availability is sparse, have lower fidelity (Bilitza et al., 2011). Nonetheless, the comparison between IRI and RIO data represents a reasonable approach to assess the overall quality of TEC measurements from the TAO buoys. Figures 12a and 12b show comparisons between the IRI-2016 model and hourly averaged RIO-12 and RIO-15 TEC data, respectively. The overall agreement with the IRI model is very good, with correlation coefficients of 0.902 and 0.890 for RIO-12 and RIO-15, respectively. On closer inspection, the scatter plots in Figure 12 show a difference between the daytime and nighttime comparison. The majority of low TEC values (corresponding to nighttime measurements) are located below the dashed diagonal line, meaning the nighttime RIO TEC values tend to be 2–5 TECU higher than the IRI-2016 model results. On the other hand, the daytime measurements of TEC are about 5–6 TECU lower than the IRI-2016 TEC values.

We further compare the IRI-2016 and RIO TEC measurements by computing their differences and binning the differences in magnetic local time (MLT) to examine the distributions. Figures 13a and 13b show histograms of data/model differences computed for RIO-12 and RIO-15, respectively. The shapes of both histograms suggest that there are two underlying Gaussian distributions. One distribution has a peak below zero and the other is centered above zero. This split is indeed due to the diurnal variation of TEC. Figures 13c and 13d show the histograms of RIO and IRI TEC differences binned for different MLT sectors. These figures now clearly show that the IRI-2016 underestimates the measured TEC during the nighttime (18–03 MLT) and overestimates it during the daytime (09–18 MLT).

6. Conclusions

Our ability to continuously monitor the ionosphere from the vast stretches of open water remains a technological challenge. This is a problem because oceans cover about 70% of the Earth's surface. Ocean-based ionospheric monitoring, heretofore, has not been possible due to the harsh environment and logistical challenges in deploying sensors on resource-constrained buoys. Additionally, the constant motion imparted by ocean waves to the buoy further complicates the GPS signal acquisition, tracking, and processing. Currently, there are no viable methods of receiving and processing GPS TEC information from a platform in the ocean. This leaves 7/10 of Earth without adequate observational coverage for ionospheric studies. Addressing this observational gap is particularly crucial for measuring ionospheric variability globally. In this paper, we have demonstrated the feasibility of making high fidelity GPS TEC measurements from ocean-based platforms, such as moored and mobile buoys. We describe the RIO GPS receiver, with its small SWaP design and software features, capable of operating autonomously from resource-constrained ocean surface buoys. We also present our concept of operation for the RIO receivers deployed on NOAA TAO buoys in the Pacific Ocean. The data quality and reliability from the RIO receivers on TAO buoys are comparable to those from ground-based GPS receivers. A preliminary analysis of the TEC data collected from the buoys, which are located near the magnetic equator, shows two key findings:

1. The observed TEC exhibits a clear seasonal dependence characterized by equinoctial maxima.
2. Moderate geomagnetic storms are associated with the observed daytime TEC enhancements.

This is the first time that GPS receivers have been deployed and operated in open waters for an extended period. This study serves as a proof of concept demonstration that continuous GPS TEC measurements can be reliably made from ocean buoys. In the future, small SWaP GPS receivers, such as RIO, can be (and should be) deployed on arrays of ocean buoys to complement the distributed networks of ground-based GPS receivers. The long-term vision of this work is to enable continuous and persistent observations from distributed sensors, from both ground-based and ocean platforms, to provide the much needed data to resolve and

quantify a variety of temporal and spatial scales of ionospheric variability. In summation, this study of GPS TEC measurements from the NOAA TAO buoys demonstrates that the ocean-based observation modality represents a new frontier in ionospheric remote sensing, which can open the way for new research activities in the geospace community.

Data Availability Statement

The source code of IRI-2016 model is available at <http://irirmodel.org>. The GPS L1 and L2C biases were computed using the online archives of the Crustal Dynamics Data Information System (CDDIS), NASA Goddard Space Flight Center, Greenbelt, MD, USA. <ftp://cddis.gsfc.nasa.gov/pub/gps/products/bias/>.

The GPS TEC data from TAO buoys are available at 10.5281/zenodo.3903770.

Acknowledgments

This study was supported by the Air Force Small Business Innovation Research (SBIR) contract FA9453-13-C-0035 to ASTRA. I.A. acknowledges support from Liquid Robotics Inc., Sunnyvale, CA, during the integration of RIO GPS receivers on Wave Gliders and the execution of field tests in Hawaii and Peru. TAO host buoys for the RIO deployments were provided by NOAA/NDBC.

References

Azeem, I., & Barlage, M. (2017). Atmosphere-ionosphere coupling from convectively generated gravity waves. *Advances in Space Research*, 61(7), 1931–1941. <https://doi.org/10.1016/j.asr.2017.09.029>

Azeem, I., Vadas, S. L., Crowley, G., & Makela, J. J. (2017). Traveling ionospheric disturbances over the United States induced by gravity waves from the 2011 Tohoku tsunami and comparison with gravity wave dissipative theory. *Journal of Geophysical Research: Space Physics*, 122, 3430–3447. <https://doi.org/10.1002/2016JA023659>

Billitz, D., Altadill, D., Truhlik, V., Shubin, V., Galkin, I., Reinisch, B., & Huang, X. (2017). International Reference Ionosphere 2016: From ionospheric climate to real-time weather predictions. *Space Weather*, 15, 418–429. <https://doi.org/10.1002/2016SW001593>

Billitz, D., McKinnell, L.-A., Reinisch, B., & Fuller-Rowell, T. (2011). The International Reference Ionosphere (IRI) today and in the future. *Journal of Geodesy*, 85(12), 909–920. <https://doi.org/10.1007/s00190-010-0427-x>

Buonsanto, M. (1999). Ionospheric storms—A review. *Space Science Reviews*, 88(3/4), 563–601. <https://doi.org/10.1023/A:1005107532631>

Burns, A. G., Solomon, S. C., Wang, W., Qian, L., Zhang, Y., & Paxton, L. J. (2012). Daytime climatology of ionospheric N_mF_2 and h_mF_2 from COSMIC data. *Journal of Geophysical Research*, 117, A09315. <https://doi.org/10.1029/2012JA017529>

Codrescu, M. V., Palo, S. E., Zhang, X., Fuller-Rowell, T. J., & Poppe, C. (1999). TEC climatology derived from TOPEX/Poseidon measurements. *Journal of Atmospheric and Solar - Terrestrial Physics*, 61(3–4), 281–298. [https://doi.org/10.1016/S1364-6826\(98\)00132-1](https://doi.org/10.1016/S1364-6826(98)00132-1)

Coster, A. J., Goncharenko, L., Zhang, S.-R., Erickson, P. J., Rideout, W., & Vierinen, J. (2017). GNSS observations of ionospheric variations during the 21 August 2017 solar eclipse. *Geophysical Research Letters*, 44, 12,041–12,048. <https://doi.org/10.1002/2017GL075774>

Crowley, G., Azeem, I., Reynolds, A., Duly, T. M., McBride, P., Winkler, C., & Hunton, D. (2016). Analysis of traveling ionospheric disturbances (TIDs) in GPS TEC launched by the 2011 Tohoku earthquake. *Radio Science*, 51(5), 507–514. <https://doi.org/10.1002/2015RS005907>

Crowley, G., Bust, G. S., Reynolds, A., Azeem, I., Wilder, R., O'Hanlon, B. W., et al. (2011). CASES: A novel low-cost ground-based dual-frequency GPS software receiver and space weather monitor. Portland, Oregon: Proceedings of ION GNSS.

Eastes, R. W., McClintock, W. E., Burns, A. G., Anderson, D. N., Andersson, L., Codrescu, M., et al. (2017). The Global-Scale Observations of the Limb and Disk (GOLD) mission. *Space Science Reviews*, 212(1–2), 383–408. <https://doi.org/10.1007/s11214-017-0392-2>

Forsythe, V. V., Duly, T., Hampton, D., & Nguyen, V. (2020). Validation of ionospheric electron density measurements derived from Spire CubeSat constellation. *Radio Science*, 55(1). <https://doi.org/10.1029/2019RS006953>

Hayes, S. P., Mangum, L., Picaut, J., Sumi, A., & Takeuchi, K. (1991). TOGA-TAO: A moored array for real-time measurements in the tropical Pacific Ocean. *Bulletin of American Meteorological Society*, 72, 339–347. [https://doi.org/10.1175/1520-0477\(1991\)072%3C0339:TTAMAF%3E2.0.CO;2](https://doi.org/10.1175/1520-0477(1991)072%3C0339:TTAMAF%3E2.0.CO;2)

Heelis, R. (2008). Low- and Middle-Latitude Ionospheric Dynamics Associated with Magnetic Storms. In P. M. Kintner, A. J. Coster, T. Fuller-Rowell, A. J. Mannucci, M. Mendillo, & R. Heelis (Eds.), *Midlatitude Ionospheric Dynamics and Disturbances* (pp. 51–61). Washington, DC: American Geophysical Union. <https://agupubs.onlinelibrary.wiley.com/doi/10.1029/181GM06>

Heelis, R. A. (2013). Low- and middle-latitude ionospheric dynamics associated with magnetic storms. In P. M. Kintner, A. J. Coster, T. Fuller-Rowell, A. J. Mannucci, M. Mendillo, & R. Heelis (Eds.), *Midlatitude ionospheric dynamics and disturbances* (pp. 51–61). Washington, DC: American Geophysical Union.

Immel, T. J., England, S. L., Mende, S. B., Heelis, R. A., Englert, C. R., Edelstein, J., et al. (2018). The Ionospheric connection explorer mission: Mission goals and design. *Space Science Reviews*, 214, 13. <https://doi.org/10.1007/s11214-017-0449-2> 36pp.

Komjathy, A. (1997). *Global ionospheric total electron content mapping using the global positioning system*, PhD dissertation, Tech. Rep. 188. Fredericton, NB, Canada: Department of Geodesy and Geomatics Eng., Univ. of New Brunswick.

Lei, J., Syndergaard, S., Burns, A. G., Solomon, S. C., Wang, W., Zeng, Z., et al. (2007). Comparison of COSMIC ionospheric measurements with ground-based observations and model predictions: Preliminary results. *Journal of Geophysical Research*, 112, A07308. <https://doi.org/10.1029/2006JA012240>

Lei, J., Wang, W., Burns, A. G., Yue, X., Dou, X., Luan, X., et al. (2014). New aspects of the ionospheric response to the October 2003 superstorms from multiple-satellite observations. *Journal of Geophysical Research: Space Physics*, 119, 2298–2317. <https://doi.org/10.1002/2013JA019575>

Mannucci, A. J., Tsurutani, B. T., Iijima, B. A., Komjathy, A., Saito, A., Gonzalez, W. D., et al. (2005). Dayside global ionospheric response to the major interplanetary events of October 29–30, 2003 Halloween Storms. *Geophysical Research Letters*, 32. <https://doi.org/10.1029/2004GL021467>

Mannucci, A. J., Wilson, B. D., Yuan, D. N., Ho, C. H., Lindqwister, U. J., & Runge, T. F. (1998). A global mapping technique for GPS-derived ionospheric electron content measurements. *Radio Science*, 33(3), 565–582. <https://doi.org/10.1029/97RS02707>

Noll, C. (2010). The Crustal Dynamics Data Information System: A resource to support scientific analysis using space geodesy. *Advances in Space Research*, 45(Issue 12), 1421–1440. <https://doi.org/10.1016/j.asr.2010.01.018>

O'Hanlon, B. W., Psiaki, M. L., Powell, S., Bhatti, J. A., Humphreys, T. E., Crowley, G., & Bust, G. S. (2011). CASES: A smart, compact GPS software receiver for space weather monitoring. In *Proc. of the 24th International Technical Meeting of the Satellite Division of the Institute of Navigation* (pp. 2745–2753). Portland, OR: Institute of Navigation (ION).

- Occhipinti, G., Rolland, L., Lognonne, P., & Watada, S. (2013). From Sumatra 2004 to Tohoku Oki 2011: The systematic GPS detection of the ionospheric signature induced by tsunamigenic earthquakes. *Journal of Geophysical Research: Space Physics*, *118*, 3626–3636. <https://doi.org/10.1002/jgra.50322>
- Robinson, T. R., & Beard, R. (1995). A comparison between electron content deduced from the IRI and that measured by the TOPEX dual frequency altimeter. *Advances in Space Research*, *16*(1), 155–158. [https://doi.org/10.1016/0273-1177\(95\)00116-V](https://doi.org/10.1016/0273-1177(95)00116-V)
- Saito, A., Fukao, S., & Miyazaki, S. (1988). High resolution mapping of TEC perturbations with the GSI GPS network over Japan. *Geophysical Research Letters*, *25*, 3079–3082. <https://doi.org/10.1029/98GL52361>
- Schreiner, W., Rocken, C., Sokolovskiy, S., Syndergaard, S., & Hunt, D. (2007). Estimates of the precision of GPS radio occultations from the COSMIC/FORMOSAT-3 mission. *Geophysical Research Letters*, *34*, L04808. <https://doi.org/10.1029/2006GL027557>
- Schreiner, W. S., Weiss, J. P., Anthes, R. A., Braun, J., Chu, V., Fong, J., et al. (2020). COSMIC-2 radio occultation constellation: First results. *Geophysical Research Letters*, *47*, e2019GL086841. <https://doi.org/10.1029/2019GL086841>
- Thomson, J., Gorton, J. B., Jha, R., & Trapani, A. (2018). Measurements of directional wave spectra and wind stress from a Wave Glider autonomous surface vehicle. *Journal of Atmospheric and Oceanic Technology*, *35*(2), 347–363. <https://doi.org/10.1175/JTECH-D-17-0091.1>
- Tsugawa, T., Otsuka, Y., Coster, A. J., & Saito, A. (2007). Medium-scale traveling ionospheric disturbances detected with dense and wide TEC maps over North America. *Geophysical Research Letters*, *34*, L22101. <https://doi.org/10.1029/2007GL031663>